


RESEARCH ARTICLE

Open Access



Analysis of newly discovered substances on the vulnerable Emperor Qin Shihuang's Terracotta Army figures

Xiaoxi Li¹, Wendi Yu^{2,3}, Desheng Lan^{1*}, Jing Zhao^{2*} , Jianhua Huang¹, Na Xi¹, Qiang Li², Yin Xia¹, Ping Zhou¹ and Hongjie Luo²

Abstract

In this paper, X-ray diffraction spectroscopy (XRD), Raman spectroscopy (RS), firing temperature analysis, pore size distribution analysis, Fourier infrared spectroscopy (FTIR), scanning electron microscopy-energy dispersive spectroscopy (SEM-EDS), and transmission electron microscopy (TEM) were utilized to analyze the unearthed vulnerable terracotta figures of Emperor Qin Shihuang's Terracotta Army, as well as the unknown precipitated white crystals and black substances. The results show that the firing temperature of the vulnerable terracotta figure is much lower than those of similar terracotta figures and red terracotta figures with good texture. The pore size of this kind of vulnerable pottery is smaller and the specific surface area is larger. In the pores, there is an alkaline solution containing Ca^{2+} that accounted for approximately 4.3% of the total mass of the sample. Along with the fracture of the delicate pottery matrix, the solution in the pores migrated to the fracture surface and chemically reacted with CO_2 in the air, generating a layer of white calcium carbonate crust. The black matter on the fracture surface of the vulnerable terracotta figure is mainly composed of amorphous carbon and graphitized carbon, which shows high activity under the catalysis of Fe and Ti elements and alkaline soil. The discovery and analysis of amorphous carbon, graphitized carbon, and white calcium carbonate crystals on the fracture surface of the Qin Shihuang's Terracotta Army provide a theoretical foundation for in-depth analysis of the terracotta warriors and horses' composition and structure, as well as scientific protection and restoration, and the stability of the original site display.

Keywords: Emperor Qin Shihuang's Terracotta Army, Vulnerable terracotta figures, Calcium carbonate, Amorphous carbon, Graphitized carbon

Introduction

Terracotta Army in the Mausoleum of Emperor Qin Shihuang, the first emperor in Chinese history, serves as one of the important funerary objects. It is known as "the eighth wonder of the world", "one of the greatest

discoveries in twentieth-century archaeological history", "the spiritual symbol of Chinese civilization" and so on. The Terracotta Army consists of more than 8000 terracotta warriors and horses made of clay and other ingredients, with various expressions and postures. It is the crystallization of the wisdom of the ancient Chinese people. It has also been an essential material for studying ancient politics, military, and culture because of its exquisite sculptures, large number, artistic attractiveness, and complete armaments (containing infantry, cavalry, crossbow, chariot, and commander). These well-preserved and lifelike terracotta sculptures demonstrate the development of pottery production techniques, exquisite

*Correspondence: lands2000@163.com; zhaojing@mail.sic.ac.cn

¹ Key Scientific Research Base of Ancient Polychrome Pottery Conservation, National Cultural Heritage Administration (Emperor Qin Shihuang's Mausoleum Site Museum), Xi'an 710600, People's Republic of China

² Shanghai Institute of Ceramics, Chinese Academy of Sciences, Shanghai 200050, People's Republic of China

Full list of author information is available at the end of the article

carving technology, and superb aesthetic capacity in the Qin Dynasty. It is fair to say that they are precious and extraordinary Chinese historical and cultural treasure troves with inestimable value.

At present, the Chinese archaeological team has conducted intermittent excavations of the terracotta warriors and horses. When repairing the cultural relics unearthed in the 23th excavation site (Fig. 1), one kind of unearthed pottery was found extremely vulnerable (Fig. 2a). The bodies were prone to fracture and crisp powder, which increased the difficulty of protection and repair. During the routine cleaning, cultural relics protection workers found that white crystals kept growing on the broken surfaces of these easily cracked pottery sculptures and would grow again after simple removal. Meanwhile, these white crystals were always attached to another type of black matter (Fig. 2b and c). Eight vulnerable terracotta figures have been discovered among the more than 120 cultural relics have been restored. Previous archaeological studies have not discovered these newly produced white crystals and black matter.

In recent years, the research on Emperor Qin Shihuang's Terracotta Army focused primarily on the chemical components of the matrix raw materials and processing [1–9], surface microorganisms [10–12], pigment and bonding materials of the painted layer [13–19] of the terracotta pottery by using optical microscopy, palynological analysis, neutron activation technique, rare earth elements analysis, immunofluorescence microscopy, matrix-assisted laser desorption/ionization time-of-flight mass spectrometry, and gas

chromatography-mass spectrometer. However, there have been few reports on this kind of pottery with new substances constantly formed on the surface that is prone to fracture. In this paper, X-ray diffraction spectrometry, firing temperature analysis, scanning electron microscopy-energy energy dispersive spectrometry, pore size distribution analysis, Fourier infrared spectrometry, Raman spectrometry, and transmission electron spectrometry were utilized to analyze and speculate the components and sources of white crystals and black matter by comparing the performance differences between vulnerable pottery and selected pottery with good texture. The purpose of this study is to provide a scientific foundation for the preservation and restoration of the vulnerable terracotta warriors and horses, as well as the stability of the original site presentation.

Experimental

Sample selection

One fragment, numbered QY-1, was taken from the vulnerable terracotta sculptures, with white crystals and black substances on the surface. This type of vulnerable pottery is dark gray and was fired in a reducing atmosphere [20]. Grey terracotta figure fragments (No. QY-2, QY-3) and red terracotta figure fragments (No. QY-4, QY-5, QY-6) with good texture were selected for comparative study. The excavation locations of these fragments were near the excavation location of QY-1. There was no matter precipitation on the surface of the terracotta figure fragments with good texture. All the samples lost their use function and can no longer be used



Fig. 1 Distribution of the vulnerable terracotta figures in the excavation pit 1 (in red box)



Fig. 2 The vulnerable terracotta figures and substances on them: **a** A vulnerable terracotta figure in Pit 1 restoration area; **b** white crystals on the fracture surface; **c** black substances on the fracture surface

for splicing. The compressive strength of QY-1 tested by universal testing machine is 13.2 MPa, but the compressive strength of other samples ranges from 28.8 MPa to 75.7 MPa. As illustrated in Fig. 3, the internal morphologies of various types of pottery bodies were examined using an ultra-deep field microscope.

Experimental methods and detection techniques

Microscopic morphology analysis

The Japanese KEYENCE VHX-2000 ultra-depth-of-field microscope was used to observe the micro-morphology of the pottery matrix. The instrument has 54 million pixels. Compared with the traditional optical microscope, it can realize more than 20 times the depth of field observation, focus on the sample surface with large concave-convex, and test the morphological changes of the sample surface.

The Japanese JEOL JSM-6700F scanning electron microscope-energy spectrometer was used to test the pottery samples, which were polished and plated with gold by an ion sputtering instrument. The microstructure of the vulnerable pottery sample was observed by scanning electron microscope, and the related components were determined by an energy spectrometer.

The microstructure and composition of black matter on the surface of the vulnerable pottery sample were measured by the American FEI Tecnai G2 F20 field emission transmission electron microscope. The acceleration voltage was 200 kV, and the resolution of the stem (HAADF) was 0.19 nm.

Composition and structure analysis

Composition elements of pottery samples were analyzed by German BRUKER M4 TORNADO^{PLUS} micro-region X-ray fluorescence imaging spectrometer. The instrument can detect all elements between C (6)–Am (95). Its acquisition speed is fast and the detection efficiency is high. The scanning speed was 1.3 mm/s, and the maximum pulse of the detector was 275,000 cps. The instrument voltage was set to 50 kV and the current was set to 599 μ A.

The German BRUKER D8 ADVANCE high-resolution powder X-ray diffractometer was used to test the composition and structure of pottery samples and white crystals. X-ray generator: Cu target, power 3 kW, pottery light tube; Scanning mode: θ – θ Goniometer; Detector: LYNX-EYE array detector (angular resolution 0.037°, diffraction intensity up to 10^8 cps). The test range of 2θ was $5^\circ \sim 80^\circ$.

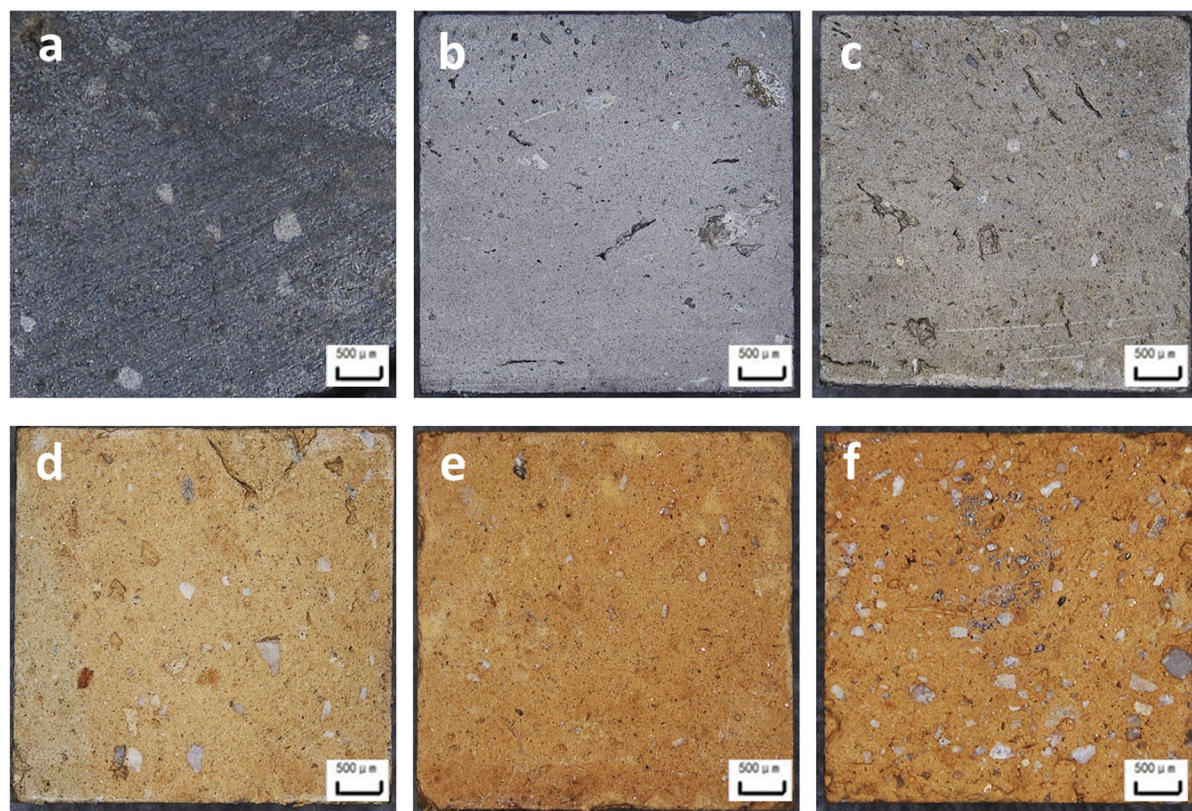


Fig. 3 Internal morphologies of various types of pottery bodies: **a** QY-1; **b** QY-2; **c** QY-3; **d** QY-4; **e** QY-5; **f** QY-6

The composition and structure of black substances on the surface of the vulnerable pottery were measured by the French HORIBA XploRA ONE micro-Raman spectrometer. The 532 nm wavelength laser was selected as the excitation light source, and the objective lens was 50 times; the spectral detection range was set to 100 ~ 2000 cm^{-1} , and the spectral resolution was 0.6 cm^{-1} .

The black matter composition of the vulnerable pottery sample was tested by the American THERMO SCIENTIFIC NICOLET IS 50 Fourier infrared spectrometer. The spectral detection range was 500 ~ 4000 cm^{-1} , the spectral resolution was better than 0.09 cm^{-1} , and the wavenumber accuracy was better than 0.01 cm^{-1} .

The American THERMO FISHER SCIENTIFIC™ DIONEX™ ICS-6000 HPIC™ system was used to test the types and concentration of soluble salt ions contained in the solution. The anion chromatographic column AS11-HC had a column length of 250 mm and a column diameter of 4 mm. The eluent was 15 mM KOH with a flow rate of 1.0 mL/min. The Cationic chromatographic column CS12A had a column length of 250 mm and a column diameter of 4 mm. The eluent was 20 mM MAS with a

flow rate of 1.0 mL/min. The chromatographic column was controlled at 30 °C.

Thermal analysis

The American TA DIL806 optical thermal dilatometer was used to test the firing temperatures of the pottery. A 20 mm * 5 mm * 5 mm ceramic block was cut from each sample for testing. The heating temperature range of the instrument was RT ~ 1400 °C, and the resolution was 50 nm and 0.1 °C. The size change of the sample was examined by measuring the shadow of the sample on the CCD detector through the shadow light method.

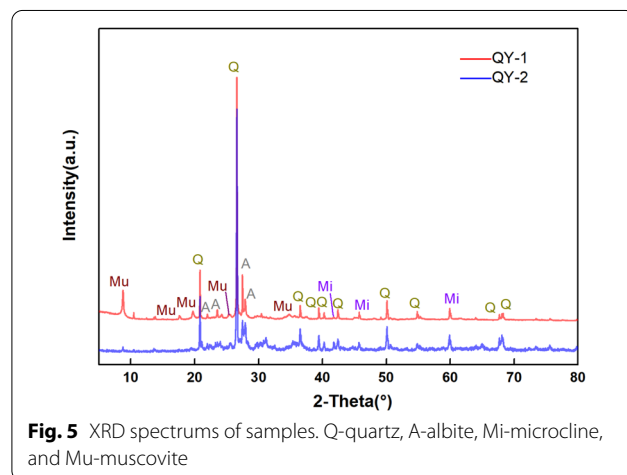
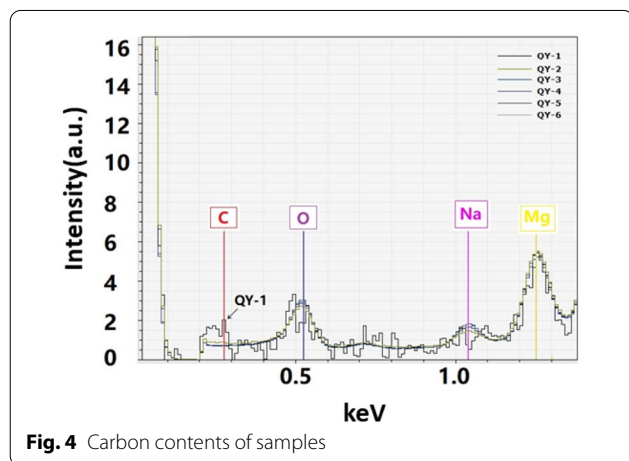
The thermogravimetric analysis of pottery samples was performed by using a German NETZSCH STA449C thermal analyzer. Under the test conditions, the nitrogen atmosphere was controlled, the temperature distribution was 25 ~ 1000 °C, and the temperature was heated at 10 °C/min.

Physical structure analysis

According to the ISO 15901-1:2005 "Pore size distribution and porosity of solid materials by mercury porosimetry and gas adsorption—Part 1: Mercury porosimetry" [21], the American Quantachrome Poremaster GT-60

Table 1 Major chemical composition elements of pottery samples (wt %)

	Na ₂ O	MgO	Al ₂ O ₃	SiO ₂	K ₂ O	CaO	TiO ₂	MnO	Fe ₂ O ₃
QY-1	0.96	2.66	19.56	58.33	4.44	1.82	0.91	0.18	10.32
QY-2	1.11	2.15	17.43	60.97	4.34	2.12	0.95	0.17	10.35
QY-3	1.08	2.09	17.67	61.73	4.82	1.64	0.91	0.16	9.52
QY-4	1.40	1.82	16.34	63.25	4.30	1.95	0.92	0.16	9.42
QY-5	1.26	2.15	17.96	60.92	4.49	1.79	0.93	0.17	10.02
QY-6	1.46	1.97	17.01	62.85	4.57	2.19	0.94	0.16	8.58

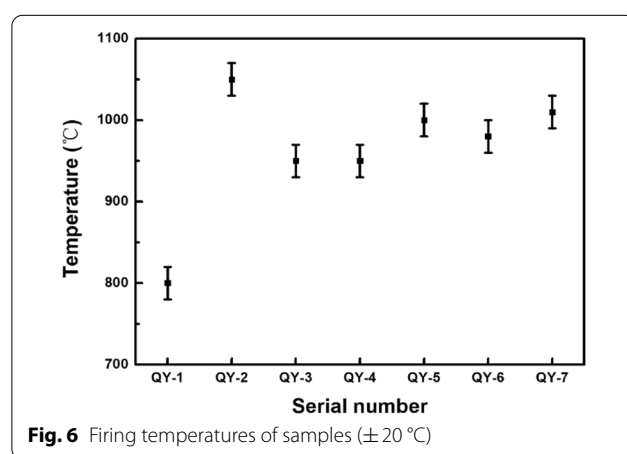


automatic mercury porosimeter (MIP) was used to test the pore size distribution ranges and physical properties of different pottery samples, with a low-pressure range of 1.5 ~ 350 kPa and a high-pressure range of 140 ~ 420 MPa. The size of the ceramic samples was 10 mm * 10 mm * 10 mm.

Results and discussion

Pottery sample performance analysis

X-ray fluorescence spectrum analysis and X-ray diffraction spectrum analysis show that there is little difference in composition between the vulnerable pottery and pottery with good texture. The main composition elements include sodium, magnesium, aluminum, silicon, potassium, calcium, titanium, manganese, and iron as determined by the XRF test (Table 1). The carbon content of the QY-1 sample is relatively higher than others (Fig. 4). Super light element micro-region X-ray fluorescence imaging spectrometer as a good detection and analysis method can distinguish the difference of carbon elements in the samples. Besides, the matrix composition of these samples is roughly the same, mainly including quartz, feldspar, muscovite, microcline, and other minerals. Specifically, XRD spectra of QY-1 and QY-2 as representatives are shown in Fig. 5.



The firing temperature values of pottery samples measured by the optical thermal dilatometer are shown in Fig. 6. The results indicate that the firing temperature of the vulnerable pottery sample QY-1 is lower, about 800 ± 20 °C, while the firing temperature of other samples is between 930 °C and 1070 °C. The most probable pore diameters of the vulnerable pottery sample QY-1 were measured by mercury porosimeter, which are mainly distributed at 0.02 μm and

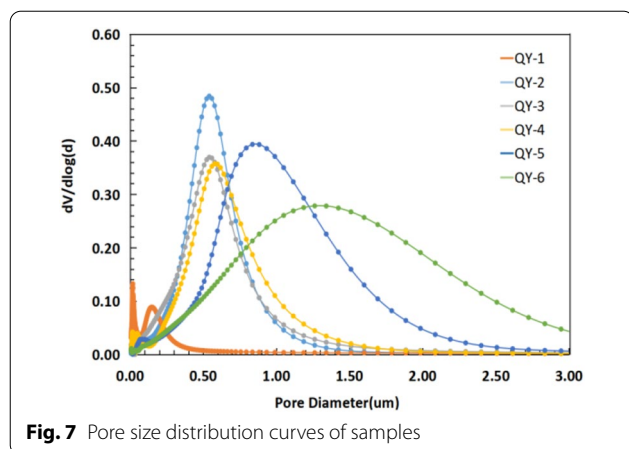


Fig. 7 Pore size distribution curves of samples

Table 2 Porosity, permeability and specific surface area of pottery samples

	Porosity (%)	Permeability (nm)	Specific surface area (m ² /g)
QY-1	23.56	7.2061e ⁻⁴	15.6574
QY-2	35.32	5.6327e ⁻²	3.6214
QY-3	30.97	2.2650e ⁻²	4.5086
QY-4	29.77	9.8372e ⁻²	6.4477
QY-5	32.59	6.066e ⁻²	2.9949
QY-6	32.97	7.0112e ⁻²	2.8765

0.16 μm . The most probable pore diameters of other samples are respectively 0.54 μm , 0.54 μm , 0.58 μm , 0.86 μm and 1.30 μm (Fig. 7). Based on the values of physical properties of pottery samples in Table 2, the overall comparisons reveal that the firing temperature of vulnerable pottery is lower, the pores are smaller, and the total pore specific surface area is larger.

Substances on the surface of the vulnerable pottery

Different from other samples, the black substances and white precipitated crystals on the fracture surface were analyzed by Raman spectrometer, scanning electron microscope-energy spectrometer, X-ray diffractometer, and transmission electron microscope, and the precipitation cause was speculated.

Analysis of black matter

The fracture surface of the vulnerable terracotta figure is unevenly distributed with black substances (Fig. 8). Raman spectrum analysis shows that the black matter has a D peak near 1350 cm^{-1} and a G peak near 1593 cm^{-1} (Fig. 9). It is generally accepted that the D peak and G peak appear in graphitized carbon materials. D peak reflects the respiratory vibration of sp^2 hybrid carbon in the ring lattice, while g peak reflects the symmetrical stretching vibration of sp^2 hybrid carbon lattice in the carbon ring or carbon chain [22]. The ratio of D peak intensity to G peak intensity ID/IG (value R) can be used to characterize the defect degree of graphitized carbon materials [23]. The greater the ratio is, the greater the disorder degree and defect degree of graphitized carbon materials. It can be seen from the comparison that the value R of the black matter is 0.89, indicating that the black graphitized carbon matter has a large degree of disorder and is rich in defects.

Moreover, it is analyzed by Fourier infrared spectroscopy that there are organic functional groups in the black matter. In Fig. 10, there is an infrared absorption peak of wide blunt spectrum peak $-\text{OH}$ with a wavenumber of $3700\sim 2500\text{ cm}^{-1}$. At 1680 cm^{-1} and 1870 cm^{-1} , it may be the $\text{C}=\text{O}$ stretching vibration peak

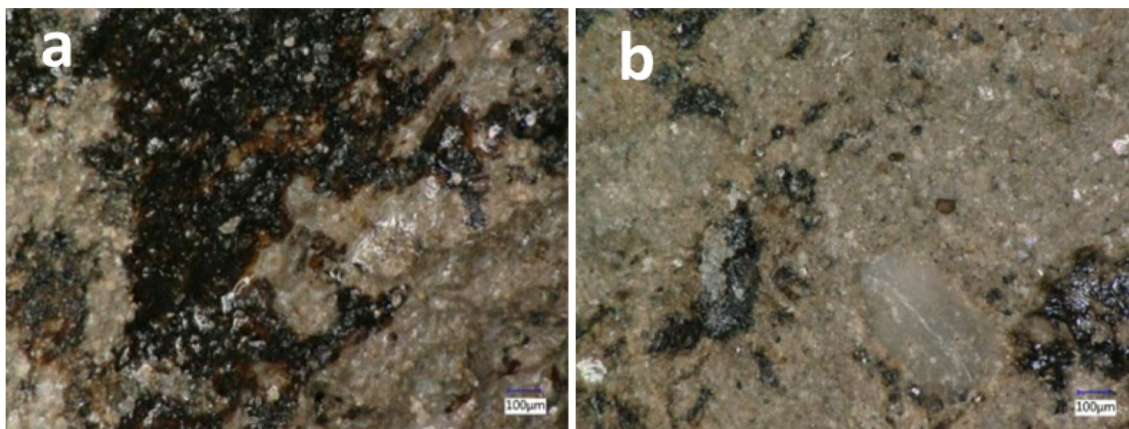


Fig. 8 Uneven black substances on the surface: **a** more black substances; **b** fewer black substances

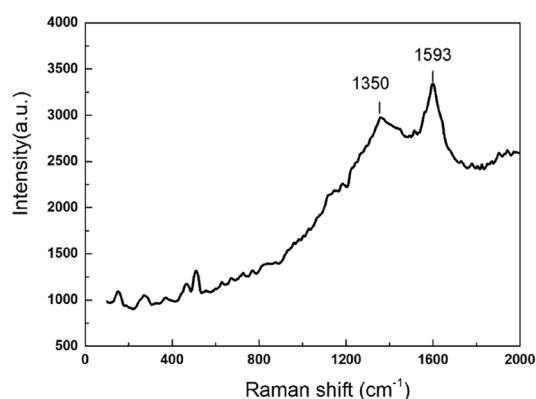


Fig. 9 Raman spectrum of black matter

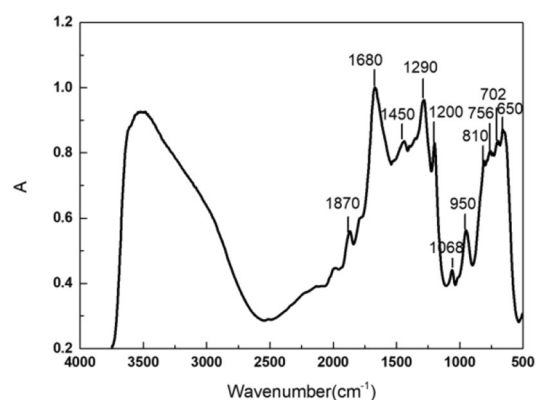


Fig. 10 Infrared spectrum of black matter

of oxygen-containing functional groups such as carboxyl, carbonyl, or ester groups. And it is the C–O stretching vibration peak at 1450 cm^{-1} and 1200 cm^{-1} . 1290 cm^{-1}

is the C–H bending vibration peak of olefins. There are C–H deformation vibration peaks at 950 cm^{-1} and 810 cm^{-1} , as well as Si–O stretching vibration peaks at 1068 cm^{-1} , 756 cm^{-1} , and 702 cm^{-1} . The existence of oxygen-containing functional groups such as –OH and C–O on the sample surface is helpful to produce more oxygen vacancy defects in the material structure and make the matter have better catalytic performance.

The test results of scanning electron micromorphology in Fig. 11 and transmission electron micromorphology in Fig. 12 show that the black matter is distributed in layers, curls, and folds, and there are nano-scale pore structures of $50\sim 100\text{ nm}$ on the surface, mainly composed of elements such as C, Al, Si, and Fe with high concentration. The distribution of C is mainly amorphous carbon and lattice striped graphitized carbon. Amorphous carbon's layered structure is disorderly and irregular, and the crystal formation is defective. Graphitized carbon forms a stacked multilayer structure, which is thin and presents a transparent tulle-like morphology. In general, the black graphitized carbon material on the surface of the terracotta figure section has a flower-like three-dimensional structure with layered curling and folding, and has the structural characteristics of graphene, which can not only restrain the collapse of graphitized carbon structure, but also increase the specific surface area of graphitized carbon material; the large specific surface area is conducive to increasing the contact between graphitized sheets and the outside, and further accelerate the reaction rate of the oxygen reduction reaction. Graphitized carbon maintains high catalytic activity and will further form the graphitized sheet due to the transition metal elements such as iron and titanium from the matrix itself and the soil, and the alkaline environment of the soil [24, 25].

The formation of black amorphous carbon and graphitized carbon on the section surface of the vulnerable

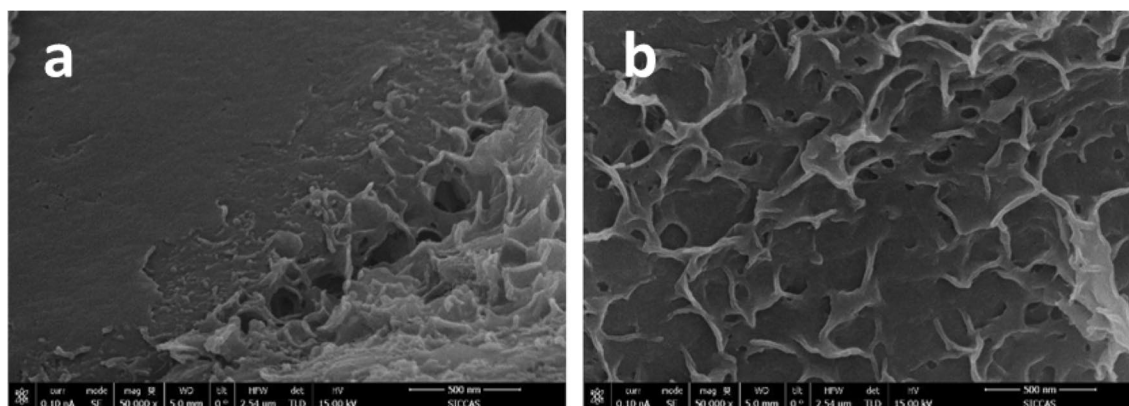


Fig. 11 SEM images of black matter: **a** formation process; **b** surface

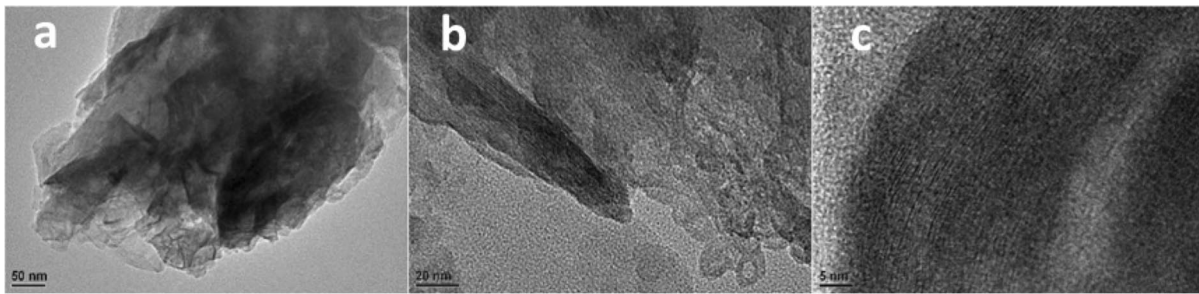


Fig. 12 TEM images of black matter in different areas (a–c)

pottery is speculated to be related to carburization. The internal carbon of the sample content is high due to the burning in reducing atmosphere or secondary incineration [26]. The vulnerable sample has a high carbon content. From the SEM–EDS results in Fig. 13, it can be seen that the carbon content in the non-black area on the surface layer and the sample interior respectively accounts for 7.63% and 8.44% of the total elements.

Analysis of white crystals

Scanning electron microscope-energy spectrometer and X-ray diffractometer were used to examine the white crystals precipitated from the vulnerable pottery sample QY-1 (Figs. 14, 15, and 16). It is determined that the main component is calcium carbonate. A salt crust with cracks is formed on the surface of the matrix. The content of Ca, C, and O respectively account for 31.7%, 7.57%, and

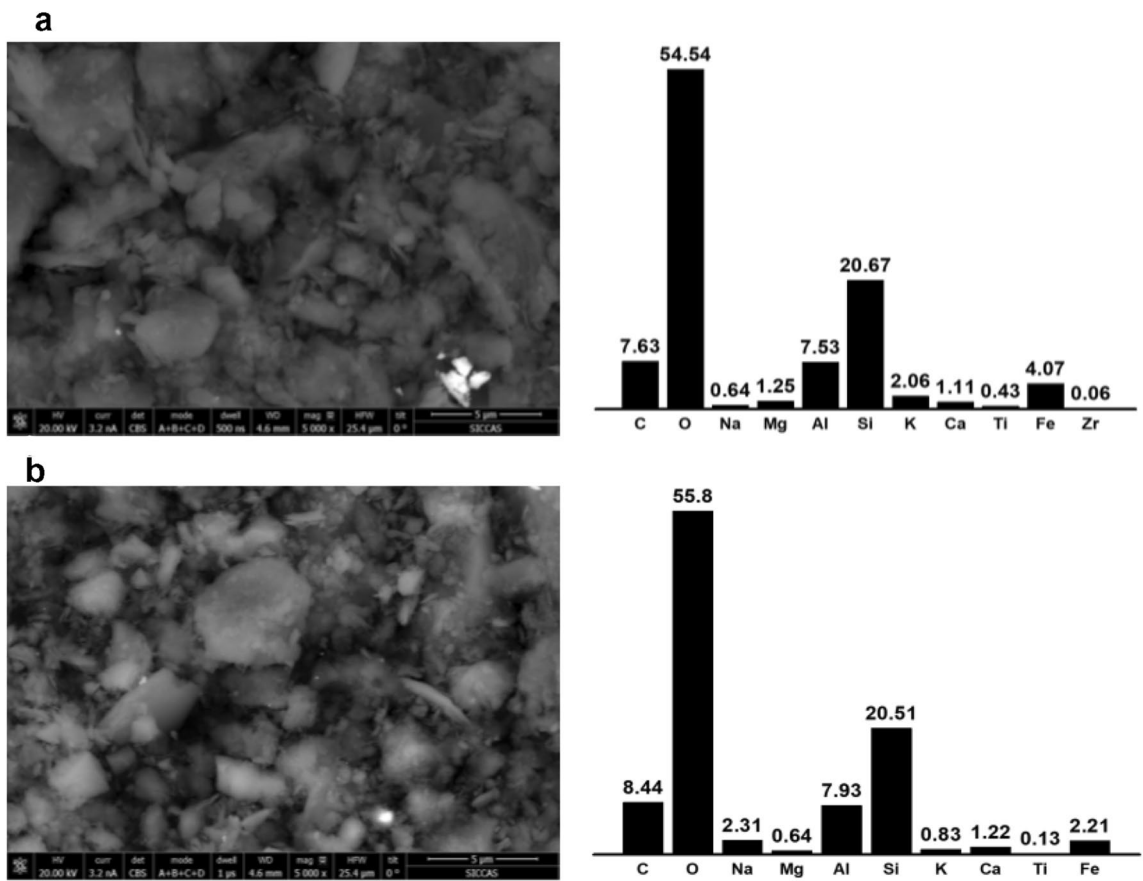


Fig. 13 SEM–EDS results of the sample: **a** non-black area on the surface layer; **b** non-black area inside



Fig. 14 White crystals morphology

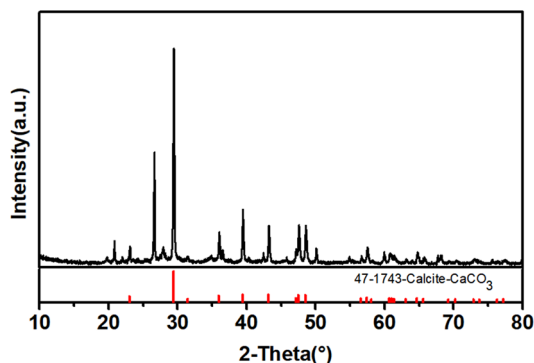


Fig. 15 XRD spectrum of white crystals

68.26% of total elements. In addition, there is also a small amount of Na, Mg, Al, Si, and Fe elements. Some Chinese efflorescent ceramics were examined and there were calcium carbonate crystals as efflorescent products [27]. It is

reasonable to infer the existence of calcium carbonate in the terracotta warriors.

A small part of the QY-1 was broken off by hands to monitor the formation of salt crystals on the sample, and the change of the fresh exposed surface was recorded in an atmosphere with temperature of 25 °C and RH of 60%. Figure 17a shows the fresh surface, while Fig. 17b shows the exposed surface after the sample has been placed for 25 days. White salt crystals grew on the new surface that was exposed to air.

The pH meter, ion chromatograph, and thermal analyzer were used to analyze the solution pH, soluble salt ions and their contents contained in the vulnerable sample and to further determine the precipitation cause of white calcium carbonate crystals. Besides, the soils (numbered as soil 1, soil 2, and soil 3) at different locations in the cultural relic burial site were selected for analysis. The results show that the buried site soil and sample contained alkaline solution with a pH value of 8.0~8.5, and the contents of Ca^{2+} were high (Table 3).

In order to assess the storage state of alkaline solution with high Ca^{2+} content in the vulnerable pottery, thermogravimetric analysis and comparison (Fig. 18) were utilized, indicating that there was a significant weight loss change in vulnerable sample QY-1 at 25~110 °C, and the lost mass accounted for about 4.3% of the total weight. It can be determined that the mass loss was due to a change in the contained solution in the sample.

Underground porous pottery contained a salt solution, and serious diseases may occur when the pottery was exposed to the air after excavation. Since the pores of the vulnerable pottery sample contained approximately 4.3% of the total weight of the sample containing Ca^{2+} alkaline solution, it is speculated that after the fracture of the vulnerable pottery sample, these

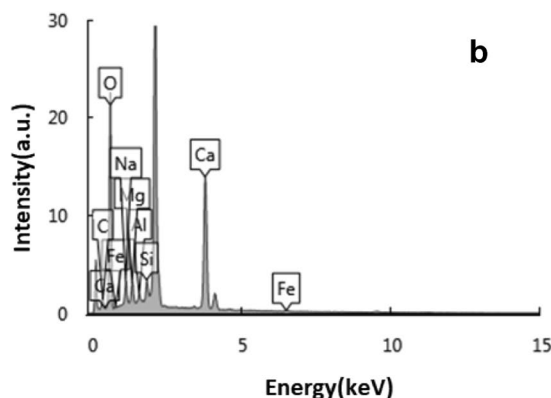
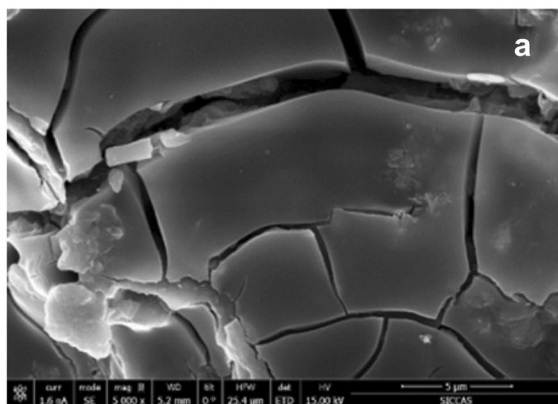


Fig. 16 Microstructure and composition analysis of white crystals: **a** cracked crust structure; **b** energy spectrum

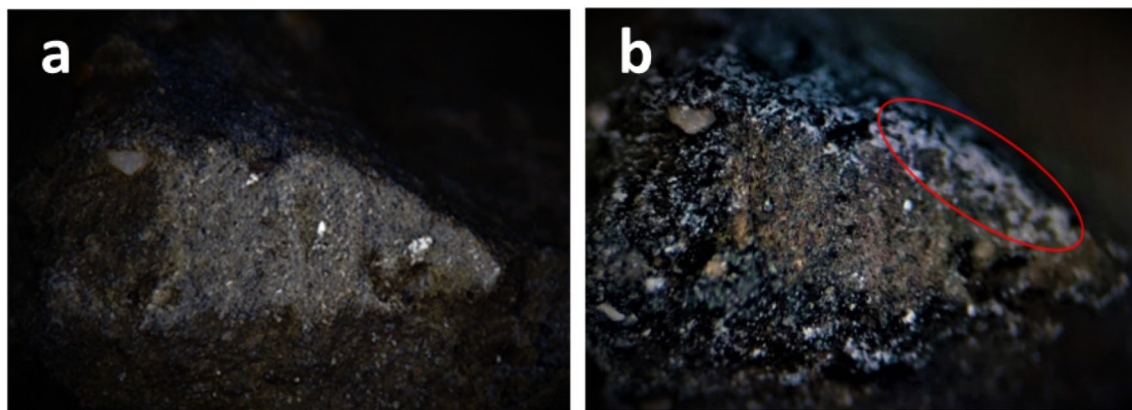


Fig. 17 Newly-growth of white crystals on the fresh exposed surface of QY-1 **a** fresh surface; **b** the surface exposed to air after 25 days

Table 3 Soluble salt ions of sample solution (mg/g)

	Na ⁺	K ⁺	Mg ²⁺	Ca ²⁺	Cl ⁻	SO ₄ ²⁻	NO ₃ ⁻
Soil 1	–	0.1246	0.0486	1.4602	0.0799	0.0903	–
Soil 2	–	0.0594	0.0079	1.9320	0.0931	0.4546	0.3878
Soil 3	–	0.0861	0.0265	1.1002	0.0298	0.2289	–
QY-1	0.0633	0.0055	0.0090	0.0722	0.0398	0.1209	0.0274

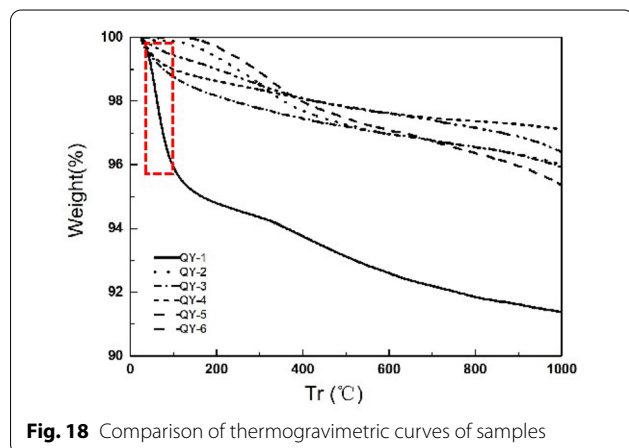


Fig. 18 Comparison of thermogravimetric curves of samples

solutions stored in the fine and dense inner pores of the pottery will continue to migrate to the fracture surface and crystallize under the action of air CO₂, forming a calcium carbonate crust.

Furthermore, the black matter which is mainly composed of amorphous carbon and graphitized carbon has excellent CO₂ adsorption due to the presence of nano-pores on its surface [28–30]. This structure will promote the combination of solution with CO₂ and

further speed the precipitation of white calcium carbonate crystals.

Conclusion

By comparing the composition, firing temperature, pore size distribution, and some physical properties of the vulnerable pottery fragment and pottery fragments with good texture of Emperor Qin Shihuang's Terracotta Army, as well as the comprehensive analysis of precipitated white crystals and black substances on the fracture surface, the main research results are as follows:

- 1) Compared with the pottery samples with good texture, the vulnerable sample QY-1 has a lower firing temperature, smaller pores, and larger total pore specific surface area. A large amount of alkaline adsorption solution containing Ca²⁺ was stored in the pores of the vulnerable sample. After the fracture of the matrix, the surface layer was exposed to the atmospheric environment to easily form white calcium carbonate crystals.
- 2) The black matter on the fracture surface is mainly composed of amorphous carbon and graphitized carbon. Graphitized carbon has a stable three-dimensional structure and electrical conductivity, and it

maintains strong catalytic activity in the presence of Fe and Ti components, and under alkaline soil conditions. Graphitized sheets will be further formed and the area will continue to increase.

- 3) It is speculated that the accumulation of more white calcium carbonate crystals on the surface of black carbon matter is related to its excellent CO₂ adsorption due to its nanometer pore structure. This structure will further promote the combination of pore solution and CO₂ and accelerate the precipitation of white calcium carbonate crystals.

The discovery and analysis of white calcium carbonate crystals, black graphitized carbon, and adsorbed alkaline solution in the vulnerable pottery of Emperor Qin Shihuang's Terracotta Army provide a scientific foundation for further restoration and protection of the cultural relics, as well as the safety and stability of the original site display.

Abbreviations

XRD: X-ray diffraction spectroscopy; RS: Raman spectroscopy; FTIR: Fourier infrared spectroscopy; SEM-EDS: Scanning electron microscope–energy dispersive X-ray spectroscopy; TEM: Transmission electron microscopy.

Acknowledgements

Not applicable.

Author contributions

XL, DL, JH, NX, YX and PZ provided experimental samples. DL and JZ defined the research project and designed the experiments. XL, WY, QL, and HL carried out the experiments. XL, WY, DL, JZ, JH and NX performed the analyses. XL and WY wrote the first draft manuscript and all co-authors discussed the results and commented on the manuscript. All authors reviewed, edited the final manuscript. All authors read and approved the final manuscript.

Funding

This work was supported by the Key Program of National Natural Science Foundation of China (51732008), National Natural Science Foundation of Shanghai in China (20ZR1422800), State Administration of Cultural Heritage (2020ZCK208), and Shaanxi key research and development program (2021ZDLSF06-01).

Availability of data and materials

All data generated or analyzed during this study are included in this published article (and its supplementary information files).

Declarations

Competing interests

The authors declare that they have no competing interests.

Author details

¹Key Scientific Research Base of Ancient Polychrome Pottery Conservation, National Cultural Heritage Administration (Emperor Qin Shihuang's Mausoleum Site Museum), Xi'an 710600, People's Republic of China. ²Shanghai Institute of Ceramics, Chinese Academy of Sciences, Shanghai 200050, People's Republic of China. ³School of Cultural Heritage, Northwest University, Xi'an 710127, People's Republic of China.

Received: 16 January 2022 Accepted: 22 April 2022
Published online: 31 May 2022

References

1. Rong B, Lan DS. Polarize light microscopy on the fragments of Qin terracotta. *Sci Conserv Archaeol*. 2005;17(3):35–9. <https://doi.org/10.16334/j.cnki.cn31-1652/k.2005.03.008>.
2. Hu YQ, Zhang ZL, Bera S, Ferguson DK, Li CS, Shao WB, Wang YF. What can pollen grains from the Terracotta Army tell us. *J Archaeol Sci*. 2006;34(7):1153–7. <https://doi.org/10.1016/j.jas.2006.10.026>.
3. Quinn PS, Zhang SX, Xia Y, Li XZ. Building the Terracotta Army: ceramic craft technology and organisation of production at Qin Shihuang's mausoleum complex. *Antiquity*. 2017;91(358):966–79. <https://doi.org/10.15184/aqy.2017.126>.
4. Li XZ, Bevan A, Martinon-Torres M, Xia Y, Zhao K. Marking practices and the making of the Qin Terracotta Army. *J Anthropol Archaeol*. 2016;42(2):169–83. <https://doi.org/10.1016/j.jaa.2016.04.002>.
5. Bevan A, Li XZ, Zhao Z, Huang JH, Laidlaw S, Xi N, Xia Y, Ma ST, Martinon-Torres M. Ink marks, bronze crossbows and their implications for the Qin Terracotta Army. *Herit Sci*. 2018;6(1):1–10. <https://doi.org/10.1186/s40494-018-0239-5>.
6. Quinn PS, Yang Y, Xia Y, Li X, Ma S, Zhang SX, Wilke D. Geochemical evidence for the manufacture, logistics and supply-chain management of Emperor Qin Shihuang's Terracotta Army, China. *Archaeometry*. 2020;63(1):40–52. <https://doi.org/10.1111/arc.12613>.
7. Li RW, Zhao WJ, Gao ZY, Li GX, Xie JZ, Guo M, Han GH, Feng SL, Fan DY, Zhang Y, Chai ZF, Zhang ZL, Zhu JX. A preliminary analysis on the development engineering and the provenance of raw material of the terracotta warriors and horses in the pits No. 2 and No. 3 of Qin Shihuang's mausoleum. *J Beijing Normal Univ*. 2004;40(3):332–7. <https://doi.org/10.3321/j.jissn:0476-0301.2004.03.009>.
8. Lei Y, Guo BF, Yuan SX. Neutron activation analysis for the provenance study on Terracotta Army of Qin Shihuang. *Nucl Tech*. 2004;27(1):38–42. <https://doi.org/10.3321/j.jissn:0253-3219.2004.01.008>.
9. Shan J, Zhou JZ, Wang CS, Qiu P, Zhang ZL, Zhu JX, Zhang YL. Preliminary study of provenance and firing style of terracotta from Qinshihuang Mausoleum. *Nucl Tech*. 2003;26(4):299–305. <https://doi.org/10.3321/j.jissn:0253-3219.2003.04.013>.
10. Luo Q, Yan SM, Li H, Du WS, Jing BW, Yang Y, Li XX, Xia Y. Research on the flocculent materials and fungi on the surface at the terracotta warrior pit No. 1 site. *Relics Museol*. 2021;38(3):101–7. <https://doi.org/10.3969/j.jissn.1000-7954.2021.03.015>.
11. Yang LJ, Tang TD, Wei XD, Zhao XF. Distribution of microorganisms in the air of hall 1 of the Qinshihuang Mausoleum. *Shaanxi Environ*. 1997;4(1):3–7.
12. Lan DS. Diseases and control of newly unearthed terracotta warriors and horses in pit No. 1 of Qinshihuang Mausoleum. *Relics Museol*. 2013;30(4):77–84. <https://doi.org/10.3969/j.jissn.1000-7954.2013.04.014>.
13. Bonaduce I, Blaensdorf C, Dietemann P, Colombini MP. The binding media of the polychromy of Qin Shihuang's Terracotta Army. *J Cult Herit*. 2008;9(1):103–8. <https://doi.org/10.1016/j.culher.2007.08.002>.
14. Xia Y, Zhou T, Zhang ZJ. Application of powdered samples polarized light microscopy in identification of artists' pigments. *Sci Conserv Archaeol*. 2004;16(4):32–5. <https://doi.org/10.16334/j.cnki.cn31-1652/k.2004.04.007>.
15. Yan HT, An JJ, Zhou T, Xia Y, Rong B. Identification of proteinaceous binding media for the polychrome terracotta army of Emperor Qin Shihuang by MALDI-TOF-MS. *Chin Sci Bull*. 2004;59(21):2574–81. <https://doi.org/10.1007/s11434-014-0372-9>.
16. Wei SY, Ma QL, Schreiner M. Scientific investigation of the paint and adhesive materials used in the Western Han dynasty polychrome terracotta army, Qingzhou, China. *J Archaeol Sci*. 2012;39(5):1628–33. <https://doi.org/10.1016/j.jas.2012.01.011>.
17. Hu WJ, Zhang K, Zhang H, Zhang BJ, Rong B. Analysis of polychromy binder on Qin Shihuang's Terracotta Warriors by immunofluorescence microscopy. *J Cult Herit*. 2015;16(2):244–8. <https://doi.org/10.1016/j.culher.2014.05.003>.
18. Yang L, Huang JH, Shen MS, Wang LQ, Wei YM. Analysis of binding media of polychrome terracotta and horses of Qin Shihuang by gas chromatography-mass Spectrometry. *Chin J Anal Chem*. 2019;47(5):695–701. <https://doi.org/10.19756/j.jissn.0253-3820.171330>.
19. Research group on color painting protection technology of the Terracotta Warriors. How to protect the colored drawings on clay figures warriors and horses buried with dead painted lacquer. *J Chin Lacquer*. 2005;26(1):7–16. <https://doi.org/10.3969/j.jissn.1000-7067.2005.01.002>.

20. Zhang ZJ. Study on the cultural relics' protection of terracotta warriors and horses in the Qin Shihuang's mausoleum. 1st ed. Xi'an: Shaanxi people's Education Press; 1998.
21. ISO 15901-1:2005: Pore Size Distribution and Porosity of Solid Materials by Mercury Porosimetry and Gas Adsorption. Part 1: Mercury Porosimetry (International Organization for Standardization, Geneva, 2005).
22. Ren RC, Zhang QW, Shi QQ, Li CX, Pang W, Dong W. Identification and analysis of amorphous graphite associated with high metamorphosed anthracite. *J China Coal Soc.* 2016;41(5):1294–300. <https://doi.org/10.13225/j.cnki.jccs.2015.1115>.
23. Zhao XS, Shi QQ, Ren RC, Zhang QW, Zhang XS. Identification of amorphous graphite based anthracite. *Bull Chin Ceram Soc.* 2016;35(3):933–7. <https://doi.org/10.16552/j.cnki.issn1001-1625.2016.03.050>.
24. Ishikawa T, Shiro Y, Cheng H. Graphite catalysis of various metal elements. *Light Element.* 1965;3(2):34–7.
25. Jin Q, Liu YL, Wu YJ, Xie CL, Xiao Y. Preparation of graphitized carbon hollow spheres by low-temperature catalytic approach. *Prog Chem.* 2012;24(1):39–46.
26. Shaanxi Institute of Archaeology and Archaeological Team of Qinshihuangling. No. 1 Brief report on trial excavation of the Terracotta Warriors in Lintong. *Cult Relics.* 1975;26(11):1–18. <https://doi.org/10.13619/j.cnki.cn11-1532/k.1975.11.001>.
27. Jin PJ, Zhang WQ, Wang QJ, Yang XG, Sun S, Fan XP, Li B. Research into water-soluble salts in efflorescent pottery during long-term storage in a museum. *Corros Sci.* 2014;89:268–74. <https://doi.org/10.1016/j.corsci.2014.09.003>.
28. Zhang YH, Li W, Ma CH, Luo S, Liu SX. Progress of research on CO₂ adsorption by porous carbon materials. *Chem Ind Forest Prod.* 2021;41(1):107–22. <https://doi.org/10.3969/j.issn.0253-2417.2021.01.015>.
29. Liu AQ, Li JJ. Research progress of carbon-based adsorbents applied in CO₂ capture. *Sichuan Chem Ind.* 2019;22(2):20–4. <https://doi.org/10.3969/j.issn.1672-4887.2019.02.007>.
30. Hang YP, Li JH, Dai G, Jia ML, Bao A. Research progress on CO₂ adsorption properties of porous solid adsorbents. *Appl Chem Ind.* 2020;49(11):2877–81. <https://doi.org/10.3969/j.issn.1671-3206.2020.11.044>.

Publisher's Note

Springer Nature remains neutral with regard to jurisdictional claims in published maps and institutional affiliations.

Submit your manuscript to a SpringerOpen[®] journal and benefit from:

- Convenient online submission
- Rigorous peer review
- Open access: articles freely available online
- High visibility within the field
- Retaining the copyright to your article

Submit your next manuscript at ► [springeropen.com](https://www.springeropen.com)